Lab on a Chip

Accepted Manuscript

ROYAL SOCIETY OF CHEMISTRY

www.rsc.org/loc

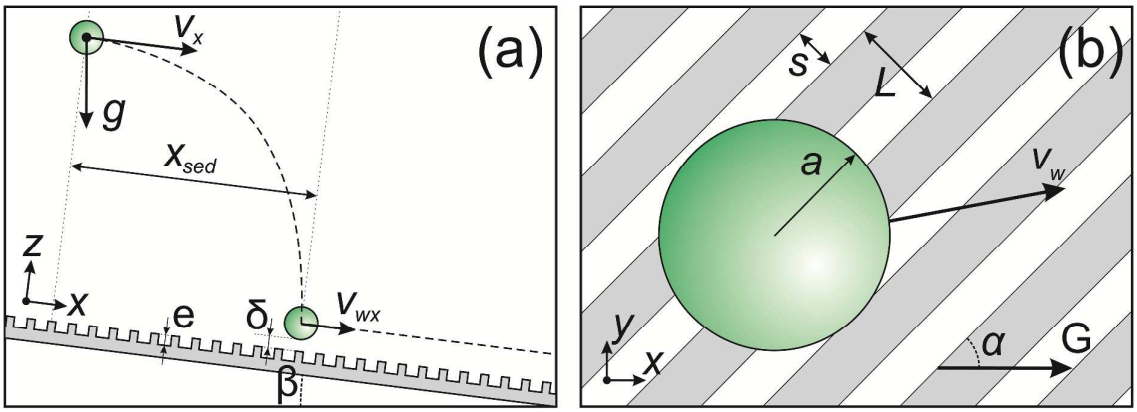

We propose a concept of fractionation of micron-sized particles in a microfluidic device with a bottom wall decorated by superhydrophobic stripe.

ARTICLE TYPE www. rsc.org/xxxxxx | XXXXXXXX

Principles of transverse flow fractionation of microparticles in superhydrophobic channels

Evgeny S. Asmolov,[a,b,c] Alexander L. Dubov,[a,d] Tatiana V. Nizkaya,[a] Alexander J. C. Kuehne,[d] and Olga I. Vinogradova*[a,d,e]

Received Xth XXXXXXXXXX 20XX, Accepted Xth XXXXXXXXX 20XX
First published on the web Xth XXXXXXXXXX 200X
DOI: 10.1039/b000000x

ABSTRACT: We propose a concept of fractionation of micron-sized particles in a microfluidic device with a bottom wall decorated by superhydrophobic stripes. Stripes are oriented at an angle α to the direction of a driving force, G, which generally includes an applied pressure gradient and gravity. Separation relies on the initial sedimentation of particles under gravity in the main forward flow, and their subsequent lateral deflection near a superhydrophobic wall due to a generation of a secondary flow transverse to G. We provide some theoretical arguments allowing us to quantify the transverse displacement of particles in the microfluidic channel, and confirm the validity of theoretical predictions in test experiments with monodisperse fractions of microparticles. Our results can guide the design of superhydrophobic microfluidic devices for efficient sorting of microparticles with a relatively small difference in size and density.

1 Introduction

Sorting of micron-sized solid particles[1] and polymer molecules,[2] isolation of biological cells or viruses from complex mixtures[3–5] are of immense importance in a variety of material science and biomedical applications. Many of these technologies belong to a class of separations known as a field-flow fractionation (FFF), where suspended particles (in a broad sense, including solid particles, fluid droplets, microcapsules or cells, typically of radius $a = 1 - 5$ μm) migrating in a microchannel are displaced perpendicular to the direction of flow under the action of external (gravity, electric, magnetic, etc) cross fields.[6,7] In the conventional FFF the external vertical force is balanced by the so-called "hydrodynamic wall-induced lift force". As a result, particles of different size, shape, density and/or surface properties migrate forward by retaining at equilibrium distances, δ, from the wall, which leads to their spreading and batch sorting in the flow direction.

In recent years, however, continuous methods in microfluidic devices have been suggested.[8,9] In these methods a horizontal external force remains perpendicular to the direction of flow, so that suspended particles spread orthogonally to it. A variety of forces, such as gravity, or electric and magnetic fields, have been used to fractionate suspensions. Some recent work suggested to use (often in addition to an external force) striped or grooved surfaces, oriented at a certain angle to the direction of flow, which could induce a deflection of the particle trajectories from the mean flow direction. There have been some theoretical[10] and experimental[5] studies, which exploit a difference in interaction of particles with chemically modified stripes. Hydrophilic grooves (Wenzel state) have been used to separate inertial particles in a relatively thin (compared to a texture period) channel.[11]

In this paper, we propose a new strategy to guide lateral fractionation of particles in microfluidic channels. We suggest to use highly anisotropic striped superhydrophobic (SH) surfaces in the Cassie state, where air is trapped by the texture. SH surfaces can induce exceptional wetting properties,[12] and, due to their superlubricating potential,[13–16] are also extremely important in the context of fluid dynamic. The effective hydrodynamic slip[17] of anisotropic SH surfaces is generally tensorial, due to a secondary flow transverse to the direction of the applied force. In the case of striped Cassie surfaces, such a transverse viscous flow[13,18,19] can be used to enhance mixing rate[20,21] in typical for microfluidic devices relatively low-Reynolds-numbers flows. Here we show, that a generation of a shear flow in the transverse direction near a bottom SH wall of the microfluidic channel results in lateral displacements of particles, sedimented under gravity, which provides a basis for

[a] *A.N. Frumkin Institute of Physical Chemistry and Electrochemistry, Russian Academy of Sciences, 31 Leninsky Prospect, 119071 Moscow, Russia*
[b] *Central Aero-Hydrodynamic Institute, 140180 Zhukovsky, Moscow region, Russia*
[c] *Institute of Mechanics, M.V. Lomonosov Moscow State University, 119991 Moscow, Russia*
[d] *DWI – Leibniz Institute for Interactive Materials, RWTH Aachen University, Forckenbeckstr. 50, 52056 Aachen, Germany*
[e] *Department of Physics, M.V. Lomonosov Moscow State University, 119991 Moscow, Russia*
* *E-mail: oivinograd@yahoo.com*

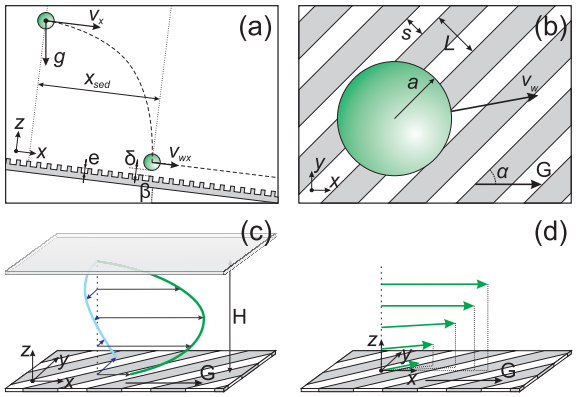

Fig. 1 Sketch of the system: side (a) and top (b) views, with a schematic of a transverse flow generation (c, d).

their efficient fractionation.*

2 General theoretical concept

We first present the theoretical basis and physical ideas underlying the approach, which we develop here to separate microparticles. We consider a flow between two parallel surfaces separated by H and inclined at an angle β as sketched in Fig. 1. The lower surface represents a striped SH (Cassie) texture of a period L and the width of the gas sectors are of s, so that the gas area fraction is $\phi = s/L$. We model the SH surface as a flat interface with no meniscus curvature, so that it appears as perfectly smooth with patterns of boundary conditions. Local slippage at the hydrophobic solid areas can be of the order of tens of nanometers.[23–27] Scalar slip lengths at the gas areas are taken as b_1 along stripes and b_2 across stripes, where the gas flux in the gas subphase becomes zero. These local slip lengths are then related to texture parameters as[28]

$$\frac{b_1}{L} \simeq \phi \frac{\mu}{\mu_g} \frac{\mathrm{erf}(3.1e/s)}{3.1}, \quad \frac{b_2}{L} \simeq \phi \frac{\mu}{\mu_g} \frac{\mathrm{erf}(2.17e/s))}{8.68}. \qquad (1)$$

Here $\mu/\mu_g \simeq 50$ is the ratio of dynamic viscosities of water and air, and e is the depth of the texture. Note that our results apply to a thick channel, $H \gg \max\{L, b_1\}$, but not to thin channels, $H \ll \min\{L, b_2\}$.[18,29] The vector $G = -\nabla p + \rho g \sin\beta$, where ρ is the density of liquid, is applied in $x-$direction at an angle α to the direction of stripes.

The starting point is the eigenvalues, $b^{\parallel}$ and $b^{\perp}$, of the effective slip lengths tensor, which correspond to the fastest (greatest forward slip) and slowest (least forward slip) directions.[17] For the striped surface they correspond to the situations when the direction x of a driving force, G, is aligned at the angle $\alpha = 0^\circ$ and 90° to the texture. For striped textures, given the area fraction and local slip lengths of the high-slip (gas) and low-slip (solid) regions, the eigenvalues of the slip-length tensor can be found numerically.[30] However, if we impose no-slip at the solid area, i.e. neglect nanometric slippage of liquid past the smooth hydrophobic surface,[23–27] which is (partly) justified provided it is much smaller than b_2, the expressions for $b^{\parallel}$ and $b^{\perp}$ take the following form:[31]

$$b^{\parallel} \simeq \frac{L}{\pi} \frac{\ln\left(\sec\left(\frac{\pi\phi}{2}\right)\right)}{1 + \frac{L}{\pi b_1} \ln\left[\sec\left(\frac{\pi\phi}{2}\right) + \tan\left(\frac{\pi\phi}{2}\right)\right]}, \qquad (2)$$

$$b^{\perp} \simeq \frac{L}{2\pi} \frac{\ln\left(\sec\left(\frac{\pi\phi}{2}\right)\right)}{1 + \frac{L}{2\pi b_2} \ln\left[\sec\left(\frac{\pi\phi}{2}\right) + \tan\left(\frac{\pi\phi}{2}\right)\right]} \qquad (3)$$

The angles $\alpha = 0$ and 90° correspond then to special directions, where $b = b^{\parallel}$ and $b = b^{\perp}$, along which fluid forces do not generate a secondary flow transverse to G, i.e. in the $y-$direction. However, in the general case of any direction α an anisotropic striped texture generates such a transverse flow, so that the flow becomes misaligned with the driving force.[17] If the stripes are inclined at an angle α to G, the forward and transverse effective slip lengths are given by[13]

$$b^{(x)} \simeq b^{\parallel} \cos^2\alpha + b^{\perp} \sin^2\alpha, \qquad (4)$$

$$b^{(y)} \simeq \frac{\sin(2\alpha)}{2}\left(b^{\parallel} - b^{\perp}\right). \qquad (5)$$

We recall that the surface textures which optimize transverse slip differs significantly from those optimizing effective forward slip. It is well known that the effective forward slip of a SH surface is maximized by increasing the gas area fraction, ϕ. In contrast, the transverse flow in SH channels is maximized by stripes with $\phi = 0.5$, where the effective slip is relatively small.[13,32]

Let us now evaluate the effective (average) slip velocities at the SH wall. We first remark that for a thick channel the fluid velocity is close to the Poiseuille velocity profile

$$u_x \simeq 4U_m\,(1 - z/H)\,z/H, \qquad (6)$$

where $U_m \simeq GH^2/(8\mu)$ is the maximal velocity, and the secondary (transverse) flow is only a small correction. Effective forward (in the $x-$direction) and transverse (in the $y-$direction) slip velocities can be then evaluated as

$$u_{sx} \simeq \frac{4U_m}{H} b^{(x)}, \qquad (7)$$

$$u_{sy} \simeq \frac{4U_m}{H} b^{(y)}. \qquad (8)$$

It immediately follows from the last equation that the velocity u_{sy} can be maximized at $\alpha = 45^\circ$ as it has been predicted before.[32] The transverse shear flow due to surface anisotropy is

* Note that this approach is conceptually different from the recent theoretical idea[22] to use hydrodynamic interactions to deflect the trajectory of particles moving along the anisotropic SH wall under an external force.

generated only in the vicinity of the SH wall and disappears far from it, which has already been observed in experiment[20] and computer simulations.[32] Since the flow rate in the $y-$direction is zero, the backward Poiseuille velocity profile should be generated as shown in Fig. 1(c):

$$u_y \simeq u_{sy}\left(1-4z/H+3z^2/H^2\right). \quad (9)$$

The effective velocity profile is then "twisted" close to the SH wall (Fig. 1(d)). The transverse component of the flow is significant only close to the SH wall.

Now consider what happens when we add particles in such SH channel. If particles enter the separation zone at the midplane of the channel, $z \simeq H/2$, their initial velocities are close to U_m. Then particles sediment under gravity (but not really stick to the wall as known from numerous FFF experiments[6,7,33]), so that they translate forward with smaller speeds and simultaneously move in y-direction. The transverse displacement then depends on their size and density since bigger and heavier particles sediment faster and, therefore, their trajectories should deflect more.

This lateral displacement can be estimated theoretically. Far from the wall the particle forward velocity is roughly equal to that of a fluid, $v_x(z) \simeq u_x(z)$, and its sedimentation rate will be constant and proportional to the Stokes settling velocity, $v_z = U_{St}\cos\beta$, where $U_{St} = 2a^2(\rho_p-\rho)g/(9\mu)$ and β is the inclination angle. Therefore, the instantaneous vertical position of the particle in an inclined channel is $z = z_0 - tU_{St}\cos\beta$ and the sedimentation time is $t_{sed} \simeq z_0/(U_{St}\cos\beta)$, where z_0 is the initial position of the particle. For particles distributed around the midplane $z_0 = H/2$ the average sedimentation length x_{sed} can be estimated as

$$x_{sed} \simeq \int_0^{t_{sed}} v_x dt = \frac{U_m H}{3U_{St}\cos\beta}, \quad (10)$$

and depends on the particle size. We note that Eq.(10) underestimates the sedimentation length, because it does not take into account the hydrodynamic interaction of particle with the wall. As a result both the sedimentation rate and the forward particle velocity decrease. More accurate estimates of v_x, v_z and x_{sed} can be obtained if we take into account the particle-wall interaction (see Appendix A). A sedimented particle continues to move with a constant velocity $(v_{xw}, v_{yw}, 0)$, which is much less than U_m. A remaining distance to the end observation window is then $d - x_{sed}$, where d is the length of the separation zone. A time $(d-x_{sed})/v_{xw}$ required to pass this distance, and therefore we obtain for a lateral displacement:

$$\Delta y \simeq \frac{v_{yw}}{v_{xw}}(d-x_{sed}). \quad (11)$$

Eq. (11) provides a basis for efficient transverse fractionation. Velocities v_{yw} are expected to be close to the slip velocity u_{sy}, and should only slightly depend on the particle size. For this reason we control the lateral displacement by choosing d and x_{sed}. Note that depending on their values two different scenarios occur. When particles have enough time to sediment - this is the situation discussed above. In this regime the required degree of separation can be attained by choosing the appropriate value of $d > x_{sed}$. However, when $d < x_{sed}$, particles will move far from the SH walls with a large velocity u_x, and it will be no lateral deflection of their trajectory from the $x-$direction of the main flow. This regime could be used to extract very small or low density particles.

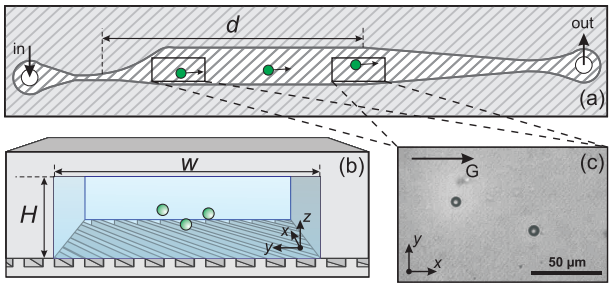

Fig. 2 (a) Sketch of the microfluidic device (top view); the boxes indicate the regions of interest at the start and end of the active separation zone of length $d = 6$ mm; (b) sketch of the active zone of a microchannel (front view); (c) typical micrograph showing 2.5 μm particles moving in the vicinity of the SH surface.

3 Microfluidic device and estimates

To illustrate the concept we perform an experimental study in a channel with a bottom striped SH wall, as sketched in Fig. 2 (a, b). The stripes are tilted at an angle $\alpha = 45^\circ$ to provide a maximal transverse flow. In most of the experiments we used a horizontal channel. However, it can be inclined up to $\beta = 45^\circ$, which allows for testing of the gravitational influence on the lateral displacement of particles. The channel are fabricated from PDMS using conventional soft lithography.[34] The smooth PDMS surfaces are slightly hydrophobic with an advancing angle $\theta_a = 115^\circ$ measured with a Drop Shape Analysis System (DSA100, Krüss, Germany). The details for preparation of smooth and grooved PDMS surfaces, and the fabrication of the channel structure are given in Appendix B. Here we only give a brief description of the channel geometry and justify the choice of the experimental parameters.

We use a grooved SH bottom wall with L =2 μm, s = 0.8 μm, and e = 1.9 μm (see Fig. 1 (a, b)) in the Cassie state, which gives effective longitudinal $\theta_a^{\parallel} \simeq 127^\circ$ and transverse $\theta_a^{\perp} \simeq 149^\circ$ advancing angles,[35] both are much larger than θ_a for a flat PDMS surface. Eq.(2) gives for this texture $b_1 \simeq 13$ μm and $b_2 \simeq 4.6$ μm. Numerical calculations[30] with typical experimental values of local slip (20-50 nm) at

the solid areas[23–27] predict for our SH texture $b^{\parallel} \simeq 170-230$ nm and $b^{\perp} \simeq 100-150$ nm, and Eq.(4) then suggests that with our α the effective forward slip is $b^{(x)} \simeq 140-190$ nm, and transverse slip is $b^{(y)} \simeq 35$ nm. Note that Eqs.(2) and (3) underestimate $b^{\parallel}$ and $b^{\perp}$, which leads to smaller $b^{(x)} \simeq 97$ nm. However, the value of a transverse slip, $b^{(y)}$, remains the same, which justifies the use of Eqs.(2) and (3) for our analysis of lateral displacements.

As a reference system we use a channel with a homogeneous flat bottom wall made from the same material, so that its (scalar) slip length, b is negligible being much smaller than $b^{(x)}$. The microchannel itself has a rectangular cross-section with a height $H = 102$ μm, which is much larger than our $b^{(x)}$. The width of the separation zone of the SH channel is very large, $w = 800$ μm, to avoid the influence of the side walls on the transverse motion of particles. The length of the separation zone is $d \simeq 6$ mm.

The microfluidic channel is connected to syringe pumps (Harvard Apparatus PHD Ultra, glass syringe Hamilton, volume 5 mL). All suspensions are injected into the channel at an equal flow rate, $Q \simeq GH^3w/(12\mu) \simeq 2U_mHw/3 \simeq 2$ μL/min, which should provide the same $U_m \simeq 650$ μm/s in all experiments and guarantee a small Reynolds number of the channel, Re$\ll 1$. The forward and transverse effective slip velocities are therefore $u_{sx} \simeq 2.5\,\mu$m/s$\ll U_m$ and $u_{sy} \simeq 0.85$ μm/s as predicted by Eqs.(7) and (8).

We use a suspension of hydrophilic silica particles with radii ranging from $a = 0.5 \pm 0.03$ to 2.5 ± 0.18 μm and a density $\rho_p = 1.8-2$ g/cm^3 (Sigma Aldrich) in milliQ water (with viscosity $\mu = 9.4 \cdot 10^{-4}$ Pa s) at a mass fractions of 0.5%. The average velocities of particles in the x-direction at a given (x,y) position are obtained by monitoring their motion in the 700 μm long observation window (see Fig. 2) using an optical microscope (Motic AE2000) equipped with a USB CCD Camera (Point Grey Flea3) with a rate of 40 frames per second. It is easy to evaluate that the sedimentation distance for small silica particles ($a = 0.5-1$ μm) should exceed d, but larger particles are expected to sediment within the channel. Then the transverse flow will provide a significant lateral displacement of large (i.e. sedimented) particles of different size (see Fig. 2 (c)).

Before our main measurements we verify the applicability of the simplified Eq.(6) for evaluation of v_x at several z in a separate experiment with fluorescently labeled silica particles (fluorescein labeled particles, Kisker Biotech GmbH& Co) with a radius of 2.5 μm. We measured the z-position of homogeneously distributed particles far from the SH wall (at several x-locations) using confocal microscopy (Leica TCS SP8) and confirm that the experimental values v_x are consistent with u_x given by Eq.(6) as shown in Fig. 3.

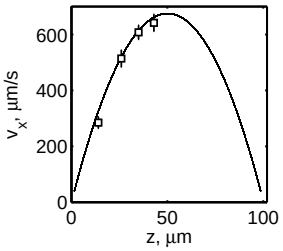

Fig. 3 Measured velocities, v_x, of fluorescently-labeled silica particles (squares) and liquid velocities, u_x, calculated with Eq.(6) (solid curve).

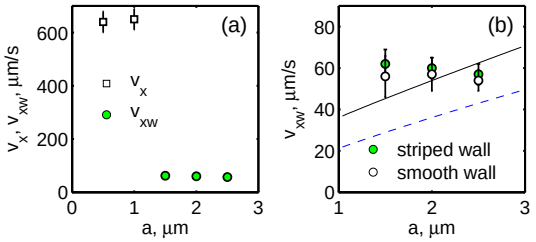

Fig. 4 (a) Forward velocities v_x (open squares) and v_{xw} (filled circles) measured at $x = 6$ mm for particles of different radii. (b) The same values for large particles (filled circles) in comparison with the velocities in the channel with the flat bottom wall (open circles). Dashed and solid lines are the predictions of the models of near-wall hydrodynamic lift[6] and of particle motion near a rough wall[36].

4 Results and discussion

We begin by studying motion of particles in the horizontal channel, $\beta = 0°$. We have first measured particle velocities at the beginning of the separation zone and found that particles of all sizes have velocities in the range from 600 to 670 μm/s, which corresponds to z-position from 35 to 65 μm, thus confirming our assumption that particles enter the channel near the mid-plane $z = H/2$. At the end of the separation zone small particles keep moving with the velocity U_m, but larger particles move with a much slower speed, $v_{xw} \simeq 60\mu$m/s$\ll U_m$, being already close to the wall (see Fig.4 (a)). This is in agreement with theoretical estimates. Indeed, Eq.(10) suggests that for particles of average radii 0.5 and 1 μm the sedimentation length is larger than d, but for larger particles x_{sed} is smaller than d. For particles of $a = 2.5$ μm we evaluate $x_{sed} \simeq 1.7$ mm and for particles of radius $a = 1.5\mu$m we obtain $x_{sed} \simeq 4.8$ mm.

Fig.4(a) shows that velocities of sedimented particles near the SH wall are independent of their size. To examine v_{xw} more closely, the data from Fig.4(a) are reproduced (in a different scale) in Fig.4(b). One conclusion from this plot is that indeed v_{xw} does not really depend on a. Also included in

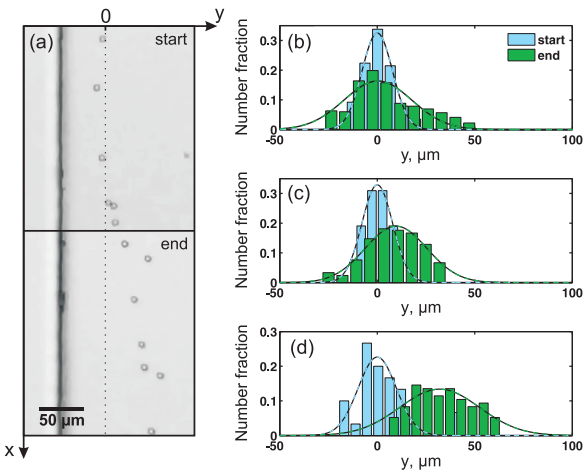

Fig. 5 Optical micrographs showing particles of radius 2.5 μm at the start and at the end of the separation zone (a); Histograms of Δy measured at $\Delta x = d$ fitted to normal distributions for particles of radius 0.5 (b), 1.5 (c) and 2.5 (d) μm.

Fig.4(b) are velocities of particles measured near the smooth wall. It can be seen that the experimental data shows velocities are slightly faster near the SH wall, but this small difference is actually within the accuracy of experiment. We conclude, therefore, that the forward slip does not really affect v_{xw}. Now, we compare our data with the model, which is usually applied in the conventional FFF, where v_{xw} was predicted to grow with a (see Appendix C).[6] One can see that the predictions of this model (dashed line in Fig. 4(b)) significantly underestimate our results, so that we have to rule out the possible effect of a "hydrodynamic wall-induced lift force" in our system. We also compare our data with predictions of the model, which quantifies the motion of particles near a rough wall[36] (see Appendix C) shown by a solid curve in Fig. 4(b). This model is more consistent with our data, but it also predicts the increase of v_{xw} with a, which we do not observe in our experiment.

We focus now on transverse particle displacements by monitoring $y-$positions of particles at the beginning and at the end of the separation zone. We first conducted this experiment in a channel with a smooth bottom wall and, as expected, found no lateral displacement of particles. Fig. 5(a) shows a typical experimental snapshot of suspensions of particles in a channel with a striped SH wall. Fig. 5(b, c, d) provides histograms of particle positions y at the start and at the end of the separation zone.[†] We see that initial particle distributions are symmetric with an average fixed to zero by choice of the coordinate system and with standard deviations σ varying from 6 to 14 μm

† For each histogram we have analyzed 200 individual particles except for a suspension of particles with radius $a = 2.5$ μm, where only 50 particles have been analyzed.

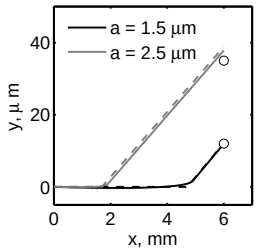

Fig. 6 Top view of trajectories of particles of radii 2.5 μm (black) and 1.5 μm (grey) calculated for $v_{yw} = 0.6\mu$m/s. Dashed curve plots predictions of Eq.(11), solid curve shows numerical results. Circles show the average experimental Δy.

for different particles. For small particles of radius 0.5 μm we observe no mean lateral displacement, i.e. mean $\Delta y = 0$ as seen in Fig. 5(b). The mean lateral displacements, Δy of larger particles are finite and depend strongly on their size. For particles of radius 1.5 μm we detect the mean $\Delta y \simeq 12$ μm, and for particles of radius 2.5 μm it is $\Delta y \simeq 35$ μm (see Fig. 5(c) and (d)) . Note that the distributions of particles spreads towards the end of the separation zone, which reflects that at the beginning our particles are distributed not only in $y-$, but also in $z-$direction.

Thus, we have measured v_{xw} and Δy independently for particles of different sizes. From this data we can deduce the transverse velocity of particles v_{yw} near the SH wall by using Eq.(11) with x_{sed} calculated with Eq.(10). The representative results are given in Table 1. Note that for all particles we found $v_{yw} = 0.6 \pm 0.1\mu$m/s, which is somewhat smaller than the theoretical value of u_{sy} discussed above. This suggests that there is additional mechanism for a dissipation in our system not included in the model (such as, for example, a meniscus curvature[37,38]). We now use experimental v_{yw} to plot in Fig. 6 the top view of calculated particle trajectories. A general conclusion from this plot is that the predictions of the simplified theory, Eq.(11), are in good agreement with numerical results (see Appendix A).

a, μm	Δy, μm	v_{xw} , μm/s	x_{sed}, mm	v_{yw}, μm/s
1.5	12	60	4.9	0.65
2.5	35	60	1.9	0.51

Table 1 Some representative experimental data.

Finally, we study the effect of gravity on the lateral displacements, by using two inclination angles of $\beta = 25^\circ$ and 45°. The results are plotted in Fig. 7. We see a significant increase in forward velocity for particles of radius 1.5 μm with the inclination angle, but not for 2.5 μm particles, which still move with v_{xw} as in Fig. 4. Calculated with Eq.(10) sedimen-

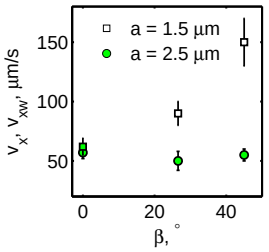

Fig. 7 Forward velocities of particles of radius 2.5 μm (filled circles) and 1.5 μm (squares) as a function of an inclination angle, β, of the microfluidic device. Filled symbols indicate v_{xw}, open symbols show v_x.

tation distances in inclined channels become larger. For particles of $a = 2.5$ μm we obtain $x_{sed} \simeq 1.9$ mm ($\beta = 25^\circ$) and $x_{sed} \simeq 2.4$ mm ($\beta = 45^\circ$) , so that they are obviously in the near-wall zone and move forward with v_{xw}. Indeed, we observe experimentally that their distribution remains very close to shown in Fig. 5(d). However, the sedimentation lengths for $a = 1.5$ μm particles become very large, and at $\beta = 45^\circ$ we get $x_{sed} \simeq 6.6 > d$ mm. In this case at the end of a separation zone $x \simeq x_{sed}$, and particles still continue to migrate with relatively high v_x without a lateral displacement. The analysis of experimental data for this suspension gives $\Delta y \simeq 0$, as expected theoretically. When $\beta = 25^\circ$ for these $a = 1.5$ μm particles we estimate that $x_{sed} \simeq 5.2$ mm, which is quite close to the outlet of the separation zone. However, it follows from the measured value of v_x that the lateral displacement of these not fully sedimented particles becomes smaller than in the horizontal channel (see Fig. 5(c)), and the detected Δy was well below 10 μm. These results demonstrate that the inclination angle of the device can be used to tune the fractionation of microparticles.

5 Conclusion

In this paper we have formulated a concept of transverse flow fractionation of microparticles, which exploits a combined effect of gravity and of a transverse hydrodynamic flow near a striped bottom SH surface of the microfluidic channel. We have predicted the transverse displacement of particles theoretically, and have generally confirmed the validity of our theory by conducting experimental measurements with monodisperse suspensions of microparticles. We have to stress, however, that the aim of our experiments was simply to illustrate a theoretical concept. For this purpose we used the optimal value of the inclination of stripes to the direction of the main flow, α, and nearly optimal value of the gas fraction, ϕ, which maximize the transverse flow, but note that we had a relatively small value of the texture period, L. Since v_{yw} and Δy scale with L (see Eqs.(2-8)), the lateral displacement can be further enhanced by using textures with larger L. Therefore, our results can guide the design of superhydrophobic microfluidic devices for efficient sorting of microparticles.

Acknowledgements

This research was partly supported by the Russian Foundation for Basic Research (grant 15-01-03069), by the DFG through SFB 985, and by the Dynasty Foundation.

A Sedimentation and trajectory of particles near the wall

The simplified model, Eq.(11), assumes that particles sediment with the Stokes velocity that their horizontal velocity coincides with that of the fluid. To calculate the sedimentation length more accurately, we have to take into account the hydrodynamic interaction of particles with the wall and use the following expressions[39,40]:

$$\begin{aligned} v_x &\simeq f(z/a-1)u_x(z), \\ v_z &\simeq U_{St}/[1+1/(z/a-1)], \\ v_y &\simeq u_y, \end{aligned} \qquad (12)$$

with the correction factor f given in[33]. Note that here we neglect some possible corrections, which could appear near a SH wall[22,41,42], since they become significant only when $z/a-1 = O(1)$. We also neglect the forward slip since $u_{sx} \ll v_{xw}$. We assume that the wall does not influence the transverse velocity of particles, so that $v_y \simeq u_y$. The trajectories, $\mathbf{x} = (x,y,z)$ are then $\mathbf{x} = \int \mathbf{v}dt$, where $\mathbf{v} = (v_x, v_y, v_z)$ is given by Eq.(12). The sedimentation length is determined from the condition $v_x(x_{sed}) = v_{xw}$, where v_{xw} is the experimental value. For $x > x_{sed}$ we use $v_x = v_{xw}$, $v_y = v_{yw}$, $v_z = 0$.

B Fabrication of microchannels

For fabrication of polydimethylsiloxane (PDMS) microchannels we use: (1) a master containing the microchannel architecture, (2) a master with the rectangular grooves and (3) a silicon wafer as a master for the flat bottom wall. The master with the grooves (2) was purchased from AMO GmbH, Germany. The microchannel master (1) was fabricated by photolithographic patterning of SU-8 (MicroChem Corp. USA) on a silicon wafer.

All the wafers are cleaned and hydrophobized with a trichloro(1H,1H,2H,2H-perfluoroocty)silane (PFOTCS, 7%, Sigma Aldrich) through the gas phase in an evacuated desiccator. PDMS replication was performed by standard procedure using Sylgard®184 Silicone elastomer KIT, Dow Corning.[35]

The geometry of the PDMS pattern was validated by field emission scanning electron microscope (Hitachi S-4800) and interference profilometry (WYKO NT2000, Veeco, USA).

To construct the closed channel geometries the microchannel structure (1) is married with either the flat bottom wall replicated from the unstructured silicon wafer (3) or with the PDMS replica of the grooves (2). To facilitate firm binding of the two PDMS layers, the individual layers were subjected to plasma treatment in an evacuated chamber with oxygen flow 30 mL/min and a plasma power of 200 W for 15 sec (PVA TePla 100 Plasma System) just before aligning and mating of the layers. Access to the closed microchannel structure is facilitated by punching holes through the thicker PDMS layer (Harris uni-core punches, Ted Pella Inc.).

C Models of particle motion near the wall

For comparison with experimental data we use two models for v_{xw}, namely, "the hydrodynamic wall-induced lift" widely accepted in FFF and the model of particle motion near a rough wall[36].

The first model[6] uses a modified equation for particle velocity, that takes into account its hydrodynamic interaction with the wall, $v_{xw} = f(\delta/a)u_x(\delta + a)$, where $\delta = z - a$ is the particle-wall distance and f is given in[33]. The value of δ is calculated by balancing the external vertical force and the lift given by $F_L = 0.172\dfrac{\mu a^3}{\delta}\dfrac{4U_m}{H}$.

The second model[36] predicts $v_{xw} = U_{St}\,g\,(\mathrm{Sh})$, where $\mathrm{Sh} = \dfrac{4aU_m}{9HU_{St}}$ is the Shields number and $g(\mathrm{Sh})$ is the fitting function valid in the range $0.04 \leq \mathrm{Sh} \leq 0.8$, which includes our values lying in the interval $0.5 \leq \mathrm{Sh} \leq 0.9$.

References

1 J. C. Giddings, *Science*, 1993, **250**, 1456–1465.
2 F. A. Messaud, R. D. Sanderson, J. R. Runyon, T. Otte, H. Pasch and S. K. R. Williams, *Progr. Polymer Sci.*, 2009, **34**, 351–368.
3 M. Fulwyler, *Science*, 1965, **150**, 1607–1626.
4 H. W. Hou, A. A. S. Bhagat, W. C. Lee, S. Huang, J. Han and C. T. Lim, *Micromachines*, 2011, **2**, 319–343.
5 S. Bose, R. Singh, M. Hanewich-Hollatz, C. Shen, C. H. Lee, D. M. Dorfman, J. M. Karp and R. Karnik, *Sci. Rep.*, 2013, **3**, 2329.
6 P. S. Williams, T. Koch and J. C. Giddings, *Chem. Eng. Commun.*, 1992, **111**, 121–147.
7 M. Martin and R. Beckett, *J. Phys. Chem. A*, 2012, **116**, 6540–6551.
8 N. Pamme, *Lab Chip*, 2007, **7**, 1644–1659.
9 P. Sajeesh and A. K. Sen, *Microfluid. Nanofluid.*, 2014, **17**, 1–52.
10 R. Zhang and J. Koplik, *Phys. Rev. E*, 2012, **85**, 026314.
11 S. Choi, T. Ku, S. Song, C. Choi and J. K. Park, *Lab. Chip*, 2011, **18**, 413–418.
12 D. Quere, *Annu. Rev. Mater. Res.*, 2008, **38**, 71–99.
13 O. I. Vinogradova and A. V. Belyaev, *J. Phys.: Condens. Matter*, 2011, **23**, 184104.
14 C. Ybert, C. Barentin, C. Cottin-Bizonne, P. Joseph and L. Bocquet, *Phys. Fluids*, 2007, **19**, 123601.
15 O. I. Vinogradova and A. L. Dubov, *Mendeleev Commun.*, 2012, **22**, 229–237.
16 J. P. Rothstein, *Annu. Rev. Fluid Mech.*, 2010, **42**, 89–109.
17 M. Z. Bazant and O. I. Vinogradova, *J. Fluid Mech.*, 2008, **613**, 125.
18 F. Feuillebois, M. Z. Bazant and O. I. Vinogradova, *Phys. Rev. E*, 2010, **82**, 055301(R).
19 S. Schmieschek, A. V. Belyaev, J. Harting and O. I. Vinogradova, *Phys. Rev. E*, 2012, **85**, 016324.
20 J. Ou, G. R. Moss and J. P. Rothstein, *Phys. Rev. E*, 2007, **76**, 016304.
21 T. V. Nizkaya, E. S. Asmolov, J. Zhou, F. Schmid and O. I. Vinogradova, *Phys. Rev. E*, 2015, **91**, 033020.
22 D. Pimponi, M. Chinappi, P. Gualtieri and C. M. Casciola, *Microfluidics Nanofluidics*, 2014, **16**, 571–585.
23 O. I. Vinogradova and G. E. Yakubov, *Langmuir*, 2003, **19**, 1227–1234.
24 C. Cottin-Bizonne, B. Cross, A. Steinberger and E. Charlaix, *Phys. Rev. Lett.*, 2005, **94**, 056102.
25 L. Joly, C. Ybert and L. Bocquet, *Phys. Rev. Lett.*, 2006, **96**, 046101.
26 O. I. Vinogradova, K. Koynov, A. Best and F. Feuillebois, *Phys. Rev. Lett.*, 2009, **102**, 118302.
27 Z. Li, L. Deramo, C. Lee, F. Monti, M. Yonger, P. Tabeling, B. Cholleta, B. Bressona and Y. Tran, *J. Fluid. Mech.*, 2015, **766**, 147–171.
28 T. V. Nizkaya, E. S. Asmolov and O. I. Vinogradova, *Phys. Rev. E*, 2014, **90**, 043017.
29 F. Feuillebois, M. Z. Bazant and O. I. Vinogradova, *Phys. Rev. Lett.*, 2009, **102**, 026001.
30 T. V. Nizkaya, E. S. Asmolov and O. I. Vinogradova, *Soft Matter*, 2013, **9**, 11671–11679.
31 A. V. Belyaev and O. I. Vinogradova, *J. Fluid Mech.*, 2010, **652**, 489 – 499.
32 J. Zhou, A. V. Belyaev, F. Schmid and O. I. Vinogradova, *J. Chem. Phys.*, 2012, **136**, 194706.
33 P. Reschiglian, D. Melucci, G. Torsi and A. Zattoni, *Chromatographia*, 2000, **51**, 87–94.
34 J. C. McDonald, A. J. R. Duffy, D. C., D. T. Chiu, H. Wu, O. J. A. Schneller and G. M. Whitesides, *Electrophoresis*, 2000, **21**, 27–40.
35 A. L. Dubov, A. Mourran, M. Möller and O. I. Vinogradova, *J. Chem. Phys.*, 2014, **141**, 074710.
36 F. Charru, E. Larrieu, J.-B. Dupont and R. Zenit, *J. Fluid Mech.*, 2007, **570**, 431–453.
37 P. Tsai, A. M. Peters, C. Pirat, M. Wessling, R. G. H. Lammertink and D. Lohse, *Phys. Fluids*, 2009, **21**, 112002.
38 E. Karatay, A. S. Haase, C. W. Visser, C. Sun, D. Lohse, P. A. Tsai and R. G. H. Lammertink, *PNAS*, 2013, **110**, 8422–8426.
39 A. J. Goldman, R. G. Cox and H. Brenner, *Chem. Eng. Sci.*, 1967, **22**, 653–660.
40 G. Barnocky and R. H. Davis, *J. Colloid Interface Sci.*, 1988, **121**, 226.
41 E. S. Asmolov, A. V. Belyaev and O. I. Vinogradova, *Phys. Rev. E*, 2011 **84**, 026330.
42 A. L. Dubov, S. Schmieschek, E. S. Asmolov, J. Harting and O. I. Vinogradova, *J. Chem. Phys.*, 2014, **140**, 034707.